



Ice nucleating properties of the sea ice diatom *Fragilariopsis cylindrus* and its exudates

Lukas Eickhoff¹, Maddalena Bayer-Giraldi², Naama Reicher³, Yinon Rudich³, Thomas Koop¹

¹Faculty of Chemistry, Bielefeld University, Universitätsstraße 25, 33615 Bielefeld, Germany

5 ²Alfred-Wegener-Institut Helmholtz-Zentrum für Polar- und Meeresforschung (AWI), Bremerhaven, Germany

³Department of Earth and Planetary Sciences, Weizmann Institute of Science, 76100 Rehovot, Israel

Correspondence to: Thomas Koop (thomas.koop@uni-bielefeld.de)

10 **Abstract.** In this study, we investigated the ice nucleation activity of the Antarctic sea ice diatom *Fragilariopsis cylindrus*.
Diatoms are the main primary producers of organic carbon in the Southern Ocean and the Antarctic sea ice diatom *F. cylindrus*
is one of the predominant species. This psychrophilic diatom is abundant in open waters and within sea ice, and it has developed
several mechanisms to cope with the extreme conditions of its environment, for example the production of ice-binding proteins
(IBP) and extracellular polymeric substances, known to alter the structure of ice. Here, we investigated the ice nucleation
15 activity of *F. cylindrus* using a microfluidic device containing individual sub-nanoliter (~90 µm) droplet samples. The
experimental method and a newly implemented Poisson statistics-based data evaluation procedure applicable to samples with
low ice nucleating particle concentrations were validated by comparative ice nucleation experiments with well-investigated
bacterial samples from *Pseudomonas syringae* (Snomax). The experiments reveal an increase of 7.2 °C in the ice nucleation
temperatures for seawater containing *F. cylindrus* diatoms when compared to pure seawater. Moreover, also *F. cylindrus*
20 fragments show ice-nucleation activity, while experiments with *F. cylindrus* ice binding protein (*fcIBP*) show no significant
ice nucleation activity. A comparison with experimental results from other diatoms suggests a universal behaviour of polar sea
ice diatoms and we provide a diatom mass-based parameterization of their ice-nucleation activity for use in models.

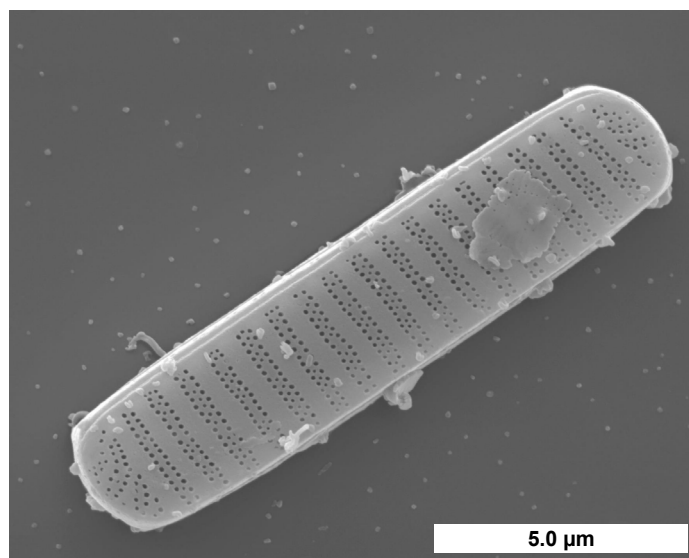
1 Introduction

Sea ice is a two-phase medium, composed predominantly of crystalline ice with embedded liquid channels and pockets
25 (inclusions) where active life can take place. As seawater freezes, dissolved sea salt ions are segregated from the growing ice
lattice and accumulate in liquid brine inclusions, which have a lower freezing point due to their high salinity. Its porous
structure makes sea ice a habitat for various organisms and enables life within the liquid brine network. Higher irradiance
levels in sea ice when compared to the seawater column represent an advantage for photosynthetically active microorganism
populating the pore space (Eicken, 1992). During sea ice formation, most microorganisms from the water column remain
30 entrapped within the ice or are scavenged by floating ice crystals (Ackley and Sullivan, 1994). Species composition changes



with the aging of ice and the stabilization of the brine channel system (Krembs and Engel, 2001), resulting in a dominance of diatom species producing “sticky” extracellular polymeric substances (EPS) with ice-adhering functions.

The diatom *Fragilariopsis cylindrus* (see Fig. 1) is widespread in polar environments and is one of the predominant species within Antarctic microbial assemblages. The species thrives within sea ice, where it can be found distributed along the sea ice column (Bartsch, 1989; Garrison and Buck, 1989; Günther and Dieckmann, 2001; Poulin et al., 2011). It is, therefore, considered as an indicator of sea ice extend in paleo-environmental studies for reconstructions of past variations (Gersonde and Zielinski, 2000). *F. cylindrus* is also abundant in the water column, for example in the proximity of the sea ice-edge zone (Kang and Fryxell, 1992; Lizotte, 2001) and in ice-covered waters (Garrison and Buck, 1989). *F. cylindrus* has developed a range of mechanism for coping with the extreme conditions occurring within sea ice (Mock et al., 2017). One prominent example is the production of so-called ice-binding proteins (IBPs) and of other EPS also found in other diatom species (Wilson et al., 2015; Aslam et al., 2018). *F. cylindrus* produces several IBP isoforms (*fc*IBPs), all of which belong to the broadly extended DUF3494 IBP family (Vance et al., 2019). It was shown that *fc*IBP isoform 11 affects the microstructure, i.e., the shape and size, of ice crystals (Bayer-Giraldi et al., 2011; Bayer-Giraldi et al., 2018). Moreover, EPS offer a protective environment to *F. cylindrus* in order to cope with the conditions of the sea ice habitat (Aslam et al., 2012a; Aslam et al., 2012b; Aslam et al., 2018). It has been suggested that *fc*IBPs accumulate in EPS and, in contact with the icy walls of brine inclusions, alter the pore space resulting in an increased habitability (Bayer-Giraldi et al., 2011).



50 **Figure 1:** *F. cylindrus* cell visualized by scanning electron microscopy. (Image courtesy of Henrik Lange and Friedel Hinz, Alfred Wegener Institute, Germany).

The very good ice-binding properties of *fc*IBP and EPS may imply that the corresponding ice-binding sites could also stabilize the formation of small ice embryos and thereby promote the nucleation of ice from liquid water (Davies, 2014; Bar Dolev et



al., 2016; Eickhoff et al., 2019; Hudait et al., 2019). The rationale behind this proposal is the fact that the active sites for ice
55 binding and those for the promotion of ice nucleation appear to be quite similar and to match those of crystalline ice (Davies,
2014; Bar Dolev et al., 2016; Eickhoff et al., 2019; Hudait et al., 2019). And indeed, it has been shown both experimentally as
well as in molecular dynamics simulations that the ice-binding antifreeze proteins of the mealworm beetle *Tenebrio molitor*
(*tmAFP*), which normally prevent the growth of existing ice crystals at temperatures just below 0 °C, can also trigger the
nucleation of new ice crystals at lower temperatures (Eickhoff et al., 2019; Hudait et al., 2019). Here, we explore whether a
60 similar ice-nucleating effect does occur also for IBPs from *F. cylindrus*.

Many particles of biological origin such as bacteria, viruses or diatoms have been detected in the sea surface microlayer as
well as in thawing permafrost (Leck and Bigg, 2005; Wilson et al., 2015; Irish et al., 2017; Creamean et al., 2020; Ickes et al.,
2020; Roy et al., 2021). Some of these biological particles are able to increase the ice nucleation temperature of small water
65 droplets and act as ice-nucleating particles INPs (DeMott et al., 2016; Ickes et al., 2020; Welti et al., 2020; Creamean et al.,
2021; Hartmann et al., 2021; Roy et al., 2021). These biologic particles can be transported to the atmospheric boundary layer
by sea spray aerosol droplets (Irish et al., 2019; Steinke et al., 2022). In the polar atmosphere, they can transported over long
distances (Šantl-Temkiv et al., 2019; Šantl-Temkiv et al., 2020). Sea spray aerosol contributes to ice nucleation under mixed-
phase cloud conditions as well as at cirrus temperatures in the upper troposphere (DeMott et al., 2016; Hartmann et al., 2021;
70 Wagner et al., 2021). Further experiments on diatoms and their EPS show that they are able to promote ice nucleation in small
droplets of water or seawater (Knopf et al., 2011; Wilson et al., 2015; Ickes et al., 2020; Xi et al., 2021). Thus, diatoms like *F.*
cylindrus may have effects on ice nucleation in cloud droplets.

2 Material and methods

2.1 Sampling and cultivation of the *F. cylindrus* diatoms

75 The investigated *F. cylindrus* cells belong to the strain TM99 isolated in 1999 from sea ice of the Weddel Sea, Antarctica, by
Thomas Mock (*Polarstern* ANT XVI/3 expedition). Stock cultures were kept in *f/2* medium (Guillard and Ryther, 1962) set
up with Antarctic water and cultivated at 0°C and under continuous illumination of approximately 25 $\mu\text{E m}^{-2} \text{s}^{-1}$. Cell numbers
were monitored using a Coulter Counter, and cells were harvested during exponential growth phase. Cell cultures were
distributed in 50 mL Falcon tubes each containing about 10^8 cells, and they were centrifuged at 0°C at 3220 g for 30 minutes.
80 The clear spent *f/2* medium was carefully separated from the cell pellet by pipetting, and both were shock-frozen in liquid
nitrogen and stored at -80°C.



2.2 Sample preparation

2.2.1 Preparation of artificial seawater

For the ice nucleation experiments, we used artificial seawater that mimics the natural conditions in the habitat of Antarctic *F. cylindrus* diatoms. The salinity in the Antarctic region is about 34.5, which corresponds to 34.5 g salts per 1000 g seawater (Roy-Barman and Jeandel, 2016), and we prepared artificial seawater of this salinity for dispersing the diatoms and as a reference for the ice nucleation experiments. For preparing the seawater, the six most important ions were considered, i.e., the cations Sodium, Potassium, Magnesium and Calcium and the anions Chloride and Sulphate, which together make up for about 99.4 % of the dissolved ions in seawater (Roy-Barman and Jeandel, 2016). The required composition was obtained by dissolving 11.8446 g (202.68 mmol) NaCl, 0.3758 g (5.04 mmol) KCl, 5.3280 g (26.21 mmol) MgCl₂·6H₂O, 4.4902 g (13.94 mmol) Na₂SO₄·10H₂O and 0.7460 g (5.07 mmol) CaCl₂·2H₂O in 477.23 g (26.49 mol) double-distilled water. More detailed information on the salts and their concentrations are given in Supplemental Information Table S1. The artificial seawater was filtered through a syringe-filter (0.22 μm, Polyethersulfone, SimplePure) in order to exclude any effect of suspended dust particles on ice nucleation. The samples were stored at a temperature of -18 °C before use.

2.2.2 Preparation of *F. cylindrus* samples

The initial *F. cylindrus* samples contained about 10⁸ diatoms per tube, see Sect. 2.1. These samples were placed in a micro reaction tube and were filled up with the filtered artificial seawater to a volume of 2 mL. The resulting stock suspension of 5×10⁷ cells per mL was used in all experiments. By further dilution with filtered artificial seawater, we generated several more dilute suspensions with concentrations of 1×10⁷, 2×10⁶, 1×10⁶ and 5×10⁵ cells per mL. For ice nucleation experiments on the fragments and exudates of the *F. cylindrus* cells, we have also filtered these five samples using a syringe-filter (0.22 μm, Polyethersulfone, SimplePure).

In order to identify the ice-nucleating entities of the *F. cylindrus* cells, we separated the different components by means of filtration and centrifugation. We filtered a 2×10⁶ cells per mL *F. cylindrus* suspension using a syringe-filter (0.22 μm, Polyethersulfone, SimplePure), such that the *F. cylindrus* cells should remain in the filter while smaller fragments of destroyed cells and any soluble species such as soluble ice-binding protein *fcIBP11* should be able to pass the filter, see Fig. S1 in the Supplemental Information for details. Thereafter, we recovered the filter cake containing the whole *F. cylindrus* cells and larger cell-fragments by shaking the filter in a vial with artificial seawater. Although we used the same volume of artificial seawater as for the preparation of the original cell suspension, we surmise that the concentration of the resuspended diatoms is lower than the initial concentration of 2×10⁶ cells per mL. Finally, the cell suspension was filtered again (0.22 μm, Polyethersulfone, SimplePure) for comparison with the pure artificial seawater sample. To verify the method all steps were also done with a vial of pure artificial seawater without suspended *F. cylindrus* cells.



115 We also performed ice nucleation experiments on fresh *f/2* medium (Guillard and Ryther, 1962) as well as on the spent *f/2*
medium, in which the *F. cylindrus* diatoms were actually grown. The sample preparation procedure is described in detail in
Supplemental Information Fig. S2. The spent *f/2* medium should not contain many cells, because they were separated by
centrifugation. Nevertheless, we filtered the medium with a syringe-filter (0.22 μm , Polyethersulfone, SimplePure), such that
only small fragments and soluble proteins (e.g., *fcIBP11*) should have remained in the filtrate. In the next step, this sample was
120 centrifuged using a 100 kDa centrifugal filter (Polyethersulfone, satorius Vivaspin 500, 15000g) such that the remaining
solution should not contain any diatom fragments but only smaller soluble molecules such as the soluble *fcIBP11* protein. For
comparison, we also applied the identical centrifugation step with freshly prepared *f/2* medium that had never been in contact
to any diatoms.

2.2.5 Preparation of *P. syringae* samples

125 In additional experiments, we verified our Poisson evaluation procedure (see Sect. 2.3.3). For this purpose, we used well-
studied bacterial cells of *P. syringae*, commercially available as Snomax[®], from the same batch as investigated in previous
studies (Budke and Koop, 2015; Wex et al., 2015). The molecular mass of the individual ice-nucleating proteins in the bacteria
is about 150 kDa (Wolber et al., 1986; Govindarajan and Lindow, 1988). A suspension of *P. syringae* with a concentration of
4 mg per mL was prepared from dry Snomax with double-distilled water. By diluting this stock suspension with further double-
130 distilled water, we also prepared additional more dilute suspensions with concentrations of 1×10^{-2} , 2×10^{-3} and 1×10^{-3} mg per
mL. Using an average value of the cell number density of 1.4×10^9 cells per mg (Wex et al., 2015), these mass concentrations
correspond to cell concentrations of 1.4×10^7 , 2.8×10^6 and 1.4×10^6 cells per mL.

2.2.6 Preparation of *fcIBP11*

Previous studies suggest that *fcIBP11* plays a major role in the response of *F. cylindrus* to freezing conditions (Bayer-Giraldi
135 et al., 2010), by binding to ice and affecting ice crystal growth (Bayer-Giraldi et al., 2011; Bayer-Giraldi et al., 2018). The
fcIBP11 protein belongs to the DUF3494 IBP family, which presently constitutes the most broadly spread IBP family often
found in sea ice microorganisms (Vance et al., 2019). For our experiments, we used the recombinant *fcIBP* isoform 11 (EMBL
Heidelberg), GenBank accession no. DR026070. The protein was expressed as previously described (Bayer-Giraldi et al.,
2011) and resuspended in Tris-HCl buffer (pH 7.0). For determining the ice nucleation activity of *fcIBP11*, we prepared a
140 stock solution with a *fcIBP11* concentration of 0.1 mmol L⁻¹. We diluted this sample by a factor of ten to a concentration of
0.01 mmol L⁻¹ using Tris-HCl buffer (pH 7.0) and performed ice nucleation experiments on both sample solutions with the
modified WISDOM microfluidic experiment (Reicher et al., 2018; Eickhoff et al., 2019), see below.



2.3 Experimental methods for ice nucleation experiments

145 2.3.1 Differential scanning calorimetry

A classic method for the investigation of homogeneous and heterogeneous ice nucleation is differential scanning calorimetry (DSC) of emulsified droplets (Rasmussen and MacKenzie, 1972; Koop, 2004). Here, we used a DSC apparatus (TA-Instruments, DSC-Q100), which was described in detail previously including its calibration procedure (Riechers et al., 2013). As bulk samples notoriously suffer from unwanted impurities, we performed measurements of inverse water-in-oil emulsion
150 samples containing micrometre-sized droplets. As many thousands of droplets are investigated simultaneously, such samples allow the detection of very reproducible exothermic heterogeneous ice nucleation signals down to the homogeneous ice nucleation temperature of about -38°C (Pinti et al., 2012; Riechers et al., 2013; Dreischmeier et al., 2017).

The principle preparation procedure for the water-in-oil emulsion (w/o) samples was almost identical to the method described earlier (Dreischmeier et al., 2017). 1 mL of 7 wt% emulsifier Span[®]65 (Merck) dissolved in 93 wt% of a mixture of 50 vol%
155 methylcyclopentane (Acros Organics, 99 %) and 50 vol% methylcyclohexane (Acros Organics, 95 %) was used as the organic phase. The aqueous phase consisted of 1 mL of an *F. cylindrus* suspension with a concentration of 1×10^7 cells per mL, see Sect. 2.2.2 above, or alternatively of 1 mL of pure artificial seawater for comparison. The mixtures of the organic and aqueous phase were subsequently emulsified by stirring with a high-speed disperser (IKA Ultra-Turrax T25 basic) for 10 min at 20'000 rpm. For a DSC measurement, about 10 mg of such an emulsion was filled into an aluminium pan that was sealed hermetically
160 and then transferred into the calorimeter. The samples were cooled at a rate of -5°C per min down to -60°C , and subsequently reheated, first at 5°C per min and then, in the temperature range between -20°C and $+5^{\circ}\text{C}$, at 1°C per min.

2.3.2 WISDOM microfluidic device

Most of the ice nucleation experiments presented in this study were carried out using droplet microfluidics. In particular, we used a microfluidic device based upon the WISDOM (Weizmann Supercooled Droplets Observation on a Microarray)
165 experiment (Reicher et al., 2018), with some minor modifications for a setup operated at Bielefeld University, including adapted temperature and heating rate calibrations, see a previous in-detail description (Eickhoff et al., 2019).

For the droplet generation, we used two syringe pumps (neMESYS NEM-B101-02 E), one filled with the aqueous sample and another with an organic phase consisting of 2 wt% Span[®]80 (Merck) dissolved in 98 wt% of a mineral oil (Sigma-Aldrich, mineral oil M3516). The microfluidic chip was connected to the pumps with PTFE tubes. The droplets generated within the
170 chip had diameters of $90\ \mu\text{m} \pm 5\ \mu\text{m}$.

For the freezing experiments, we placed the microfluidic chip after the droplet production on a temperature-controlled cold-stage (Linkam, BCS 196) attached to an optical microscope (Olympus, BX51 TRF). The temperature of the droplets in the chip was calibrated with respect to the cooling (or heating) rate as well as to the absolute temperature, and is described in detail in a previous study (Eickhoff et al., 2019). The freezing of the droplets was observed using the transmission mode of the
175 microscope and we recorded the images with a digital camera (Q-Imaging, MicroPublisher 5.0 RTV) for later analysis by a



LabView routine that detects a freezing event from the change in grey values of a particular droplet upon freezing. Typical changes in the droplets' grey values during freezing experiments are depicted in Supplemental Information Fig. S3. In each individual experiment, between about 45 to 70 droplets were observed simultaneously, depending upon the percentage of droplet-filled microcells within the droplet array of the chip.

180 For all *F. cylindrus* measurements, the chip was first cooled to a temperature of -20 °C at a rate of -5 °C per min, because no freezing events were detected in this temperature range. After equilibration at this temperature for 2 min, the samples were then cooled at a slower rate of -1 °C per min to -45 °C, at which all droplets were frozen. Thereafter, the chip was heated relatively quickly at a rate of 5 °C per min, until -10 °C, and after two minutes of equilibration, it was then heated to 5 °C at 1 °C per min. The detailed temperature profiles for each type of experiment are listed in Supplemental Information Table S2.

185 2.3.3 Evaluation procedure for samples with small INP concentrations

Ice nucleation studies using droplet arrays usually employ high concentrations of INPs, e.g. mineral dust particles or bacterial cells, with a large number of INPs per droplet (Budke and Koop, 2015; Hiranuma et al., 2015; Wex et al., 2015; DeMott et al., 2018; Hiranuma et al., 2019; Kunert et al., 2019; Ickes et al., 2020).

In the present study, the INP concentrations were much lower due to the limited availability of *F. cylindrus* cells. We investigated droplets with a diameter of 90 µm, corresponding to a volume of about 380 pL. As the concentrations c of *F. cylindrus* cells varied between 5×10^5 and 5×10^7 cells mL⁻¹, the corresponding average INP concentrations were between about only 0.19 up to 19 cells per droplet. It becomes immediately clear that when the average INP concentration λ is smaller than 1, i.e. less than one cell per droplet, there must be droplets devoid of any cells, because the number of cells in an individual droplet can only be an integer (assuming only whole cells – without fragments – being present). In such a case, heterogeneous ice nucleation cannot be triggered in every droplet, but only in those containing at least one cell. Hence, homogeneous ice nucleation is to be expected to occur in the 'empty' droplets. Moreover, even if the average INP concentration λ is exactly one per droplet, there will be a few droplets that contain two or more INPs and, thus, other droplets that do not contain any INPs. The distribution of INPs among microfluidic droplets at small average INP concentration can be described using Poisson statistics (Huebner et al., 2007; Köster et al., 2008; Edd et al., 2009; Collins et al., 2015). The following Poisson distribution can be used to describe the probability $P_\lambda(k)$ that an individual droplet contains exactly k INPs when the average concentration is λ INPs per droplet:

$$P_\lambda(k) = \frac{\lambda^k}{k!} \exp(-\lambda). \quad (1)$$

Note that the derivation of the Poisson distribution contains a simplification that require a larger number of droplets and hence Eq. (1) becomes more accurate as the number of investigated droplets increases. For the microfluidic experiments performed in this work with more than a hundred droplets investigated for each sample the simplification applies.



The average number of INPs per droplet, λ , is easily calculated from the concentration c of INPs in the stock solution and the volume V of an individual microfluidic droplet:

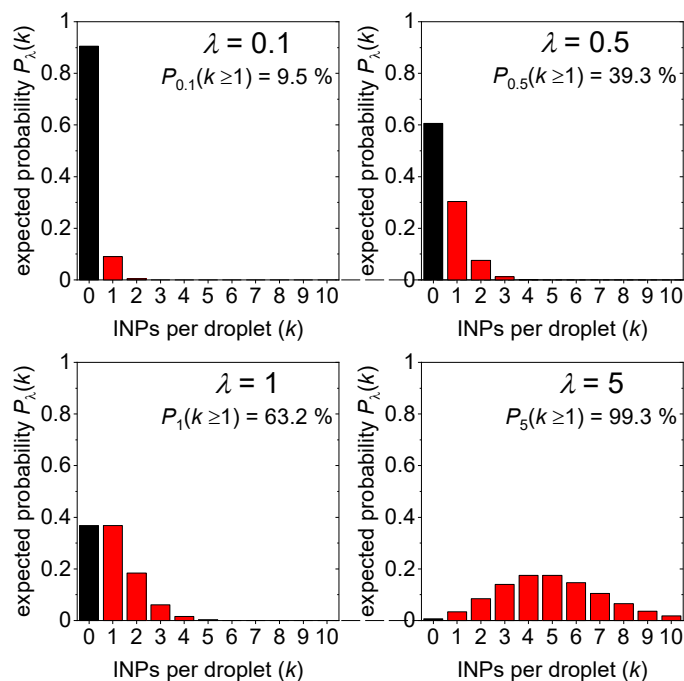
$$\lambda = c \cdot V_{\text{drop}} . \quad (2)$$

Furthermore, the droplet volume V_{drop} can be expressed by the droplet's radius r or alternatively by its diameter d :

$$210 \quad V_{\text{drop}} = \frac{4}{3}\pi \cdot r^3 = \frac{1}{6}\pi \cdot d^3 . \quad (3)$$

Figure 2 shows the calculated Poisson distributions of the number of cells per droplet for four different values of λ in a concentration range relevant to this study. For lower values of λ , the histograms exhibit the tilted shape typical of Poisson distributions, while for larger values of λ , the Poisson distribution approaches the more symmetrical shape of a normal distribution (Koop et al., 1997).

215



220 **Figure 2:** Calculated probability $P_\lambda(k)$ of the number k of INPs per droplet for different values λ of the average cell concentration per droplet. The black-coloured bars indicate the probability for the occurrence of droplets without any INPs, while the red-coloured bars indicate the combined probability $P_\lambda(k \geq 1)$ for droplets containing at least one INP. The corresponding values for $P_\lambda(k \geq 1)$ are annotated in each panel for different values of λ .

For the ice nucleation experiments considered here, only those droplets containing at least one INP and those without any INPs are relevant, as this determines whether they are subject to heterogeneous or homogeneous nucleation, respectively. Whether a droplet contains one, two or more INPs is of less importance, as long as every INP is identical and, thus, induces



225 heterogeneous ice nucleation at the same temperature. The probability that a droplet does not contain any INPs can be calculated easily by inserting $k = 0$ into Eq. (1):

$$P_{\lambda}(0) = \frac{\lambda^0}{0!} \exp(-\lambda) = \frac{1}{1} \exp(-\lambda) = \exp(-\lambda). \quad (4)$$

$P_{\lambda}(0)$ is shown as the black-coloured bar in each panel of Fig. 2. The probability that a droplet contains at least one INP, $P_{\lambda}(k \geq 1)$, is given by the combined probability of all red-coloured bars in each panel of Fig. 2, and it can be calculated
230 using the fact that the sum of all probabilities $P_{\lambda}(k)$ for k from 0 to ∞ must become 1 (see Eq. (5)):

$$P_{\lambda}(k) = \sum_{k=0}^{\infty} \frac{\lambda^k}{k!} \exp(-\lambda) = 1. \quad (5)$$

Hence, $P_{\lambda}(k \geq 1)$ can be calculated from the following difference

$$P_{\lambda}(k \geq 1) = \sum_{k=1}^{\infty} \frac{\lambda^k}{k!} \exp(-\lambda) = \sum_{k=0}^{\infty} \frac{\lambda^k}{k!} \exp(-\lambda) - \sum_{k=0}^0 \frac{\lambda^k}{k!} \exp(-\lambda) = 1 - P_{\lambda}(0) = 1 - \exp(-\lambda). \quad (6)$$

Since λ can be expressed by the product of the droplets' diameter and the known concentration of INPs in the stock solution,
235 c , (see Eq. (2) and Eq. (3)) this yields:

$$P_{\lambda}(k \geq 1) = 1 - \exp\left(-\frac{\pi}{6} \cdot c \cdot d^3\right). \quad (7)$$

The equations above have been derived for applications where the average concentration c of INPs in solution is known. However, in ice nucleation experiments of natural samples, the concentration c of INPs per volume is often unknown a priori and other values such as the organic carbon content has to be used for comparison (Gute and Abbatt, 2020; Xi et al., 2021). In
240 such cases, Eq. (7) can be used to obtain a rough estimate of λ and, thus, c from ice nucleation experiments when a plateau in the experimental frozen fraction curve is observed. The frozen fraction is defined as the number of frozen droplets relative to the number of all droplets, at a given temperature (Budke and Koop, 2015). Here, we term the value of the frozen fraction at the plateau as f'_{ice} . If a sufficiently large number of droplets is investigated, then f'_{ice} corresponds to the fraction of droplets that froze heterogeneously and thus may be equated with that fraction of droplets containing at least one INP.

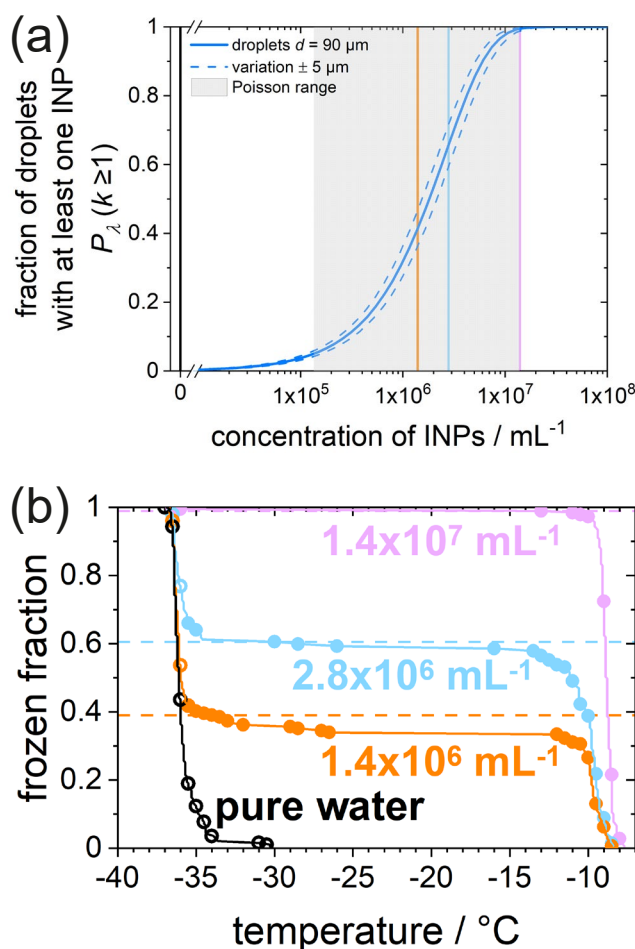
245 There are two underlying assumptions for experimentally obtaining f'_{ice} . First, every droplet containing at least one INP freezes heterogeneously, which appears entirely reasonable. Secondly, every droplet containing one or more INPs freezes at a higher temperature than those droplets without any INP, i.e. the difference between the heterogeneous and homogeneous ice nucleation temperature is large enough to be easily distinguished in the experiment. With these two assumptions a plateau in the frozen fraction curve can be interpreted as follows: the fraction of droplets below the plateau froze heterogeneously and
250 contain at least one INP, and the fraction of droplets above the plateau froze homogeneously (when their freezing temperature is consistent with homogenous freezing) and, thus, do not contain INPs. In practise, this evaluation procedure does not work if none of the droplets froze heterogeneously or if all droplets froze heterogeneously at the same temperature without any



obvious plateau, i.e. it is only applicable for intermediate average INP concentrations in what we term the “Poisson relevant range”.

255 We define this “Poisson relevant range” as the range of average INP concentrations, in which both droplets without any INP as well as droplets containing one or more INPs occur and, thus, both can be observed readily in the corresponding freezing experiments. For the experiments presented here, we establish the Poisson relevant range as the area between $P_\lambda(k \geq 1)$ values of 5.0 % and 99.5 %. The lower limit was set at 5.0% in order to avoid any influence of the freezing of a minor fraction of droplets induced by impurities, the upper limit corresponds to about one out of 200 droplets not containing any INP and thus
260 freezing homogeneously. For higher concentrations, when every droplet contains at least one INP, the above Poisson evaluation is not needed and the classic method can be used, and so this upper limit sets an endpoint for the Poisson-based evaluation. The classic method indeed assumes that every observed droplet contains at least one INP and it has been described in detail previously (Murray et al., 2012; Budke and Koop, 2015).

To demonstrate the concentration range suitable for the Poisson method, i.e. the Poisson relevant range, the latter is indicated
265 in Fig. 3a as the grey shaded area. The solid blue curve shows the values of $P_\lambda(k \geq 1)$ calculated using Eq. (7) as a function of the average INP concentration c of the studied sample and a droplet diameter of 90 μm . The two dashed lines show the changes for a deviation of $\pm 5 \mu\text{m}$ in droplet diameter.



270 **Figure 3: (a)** Fraction of droplets containing at least one INP, $P_\lambda(k \geq 1)$ as a function of INP concentration in the investigated *P. syringae*
 sample. The solid blue curve represents the values of $P_\lambda(k \geq 1)$ for the droplets in the WISDOM experiment with a diameter of $90 \mu\text{m}$,
 calculated using Eq. (7), the dashed curves indicate the uncertainty for a variation of $\pm 5 \mu\text{m}$ in droplet diameter. Eq. The grey shaded area
 shows the Poisson relevant range, with the lower and upper limits at the concentrations corresponding to $P_\lambda(k \geq 1) = 0.050$ and $P_\lambda(k \geq 1)$
 = 0.995, respectively. The coloured vertical bars mark the experimentally investigated concentrations of *P. syringae*: $1.4 \times 10^6 \text{ mL}^{-1}$ (orange),
 275 $2.8 \times 10^6 \text{ mL}^{-1}$ (blue), and $1.4 \times 10^7 \text{ mL}^{-1}$ (purple) and pure water (black). A comparable plot for the *F. cylindrus* diatoms can be found in
 Fig. S4. **(b)** Fraction of frozen droplets as a function of temperature for different concentrations of *P. syringae* bacteria in double-distilled
 water (coloured) and pure double-distilled water (black) for reference. The horizontal lines mark the values for $P_\lambda(k \geq 1)_{\text{measured}}$, see text.
 Data points of frozen fractions are binned in temperature intervals of $0.5 \text{ }^\circ\text{C}$ (intervals without freezing events are not shown). Filled circles
 represent droplets containing *P. syringae* cells (based on calculations for $P_\lambda(k \geq 1)$ with Eq. (7)), in which freezing was induced
 280 heterogeneously. Open circles represent droplets that should not contain *P. syringae* according to the calculations and, thus froze
 homogeneously.

To verify the procedure, we investigated aqueous suspensions of the well-studied ice-nucleating bacterium *Pseudomonas syringae* in the form of the commercial product Snomax (Morris et al., 2011; Budke and Koop, 2015; Wex et al., 2015). The ice nucleation temperatures of each about 165 ± 15 droplets, from three single measurements with 45 to 70 droplets each,



285 containing either pure double-distilled water or three different concentrations of *P. syringae* were investigated, see
Supplemental Information Table S3. These concentrations are also marked in Fig. 3a as vertical lines. A similar plot for the *F.*
cylindrus diatoms can be found in Fig. S4. The resulting experimental frozen fraction curves of *P. syringae* are shown in Fig.
3b. Double-distilled water (black open symbols) shows a steep increase in frozen fraction below about $-34.0\text{ }^{\circ}\text{C}$, in agreement
with homogeneous ice nucleation rates of droplets of such diameter (Koop and Murray, 2016; Reicher et al., 2018; Eickhoff
290 et al., 2019). Following this observation, all droplets of the *P. syringae* samples that froze at around or below this temperature
are assumed to have nucleated homogeneously, i.e. they are considered to contain no INPs in the analysis below.

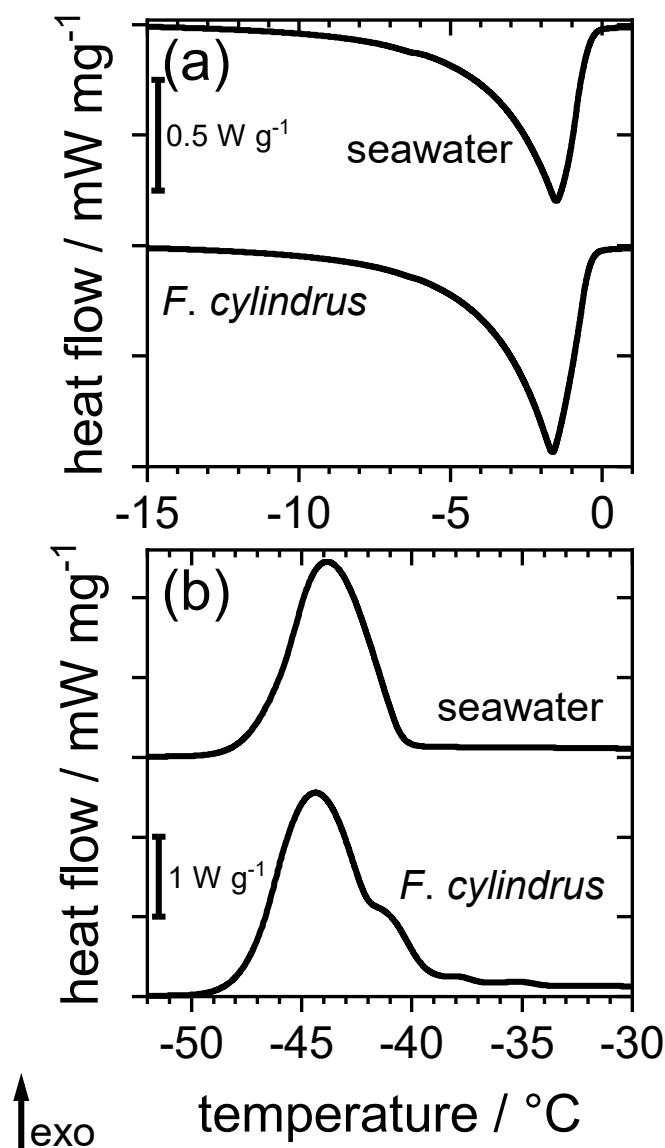
For all *P. syringae* samples, the first freezing events occur at much higher temperatures of about -8 to $-9\text{ }^{\circ}\text{C}$, and the frozen
fraction curve in each case initially increases strongly before reaching a plateau, and subsequently the remaining liquid droplets
freeze only at very low temperatures. In each sample, the plateau occurs at a different value of the frozen fraction, e.g. f'_{ice} is
295 higher the larger the *P. syringae* concentrations (pink > blue > orange). We determined the corresponding f'_{ice} values, as
defined above, from the experimentally obtained frozen fraction curve as the value of the frozen fraction at $-34.0\text{ }^{\circ}\text{C}$, i.e. at the
threshold between heterogeneous and homogenous ice nucleation as defined above. The resulting f'_{ice} values for the three
concentrations were 0.99, 0.61, and 0.39, respectively, indicated as the dashed horizontal lines in Fig. 3b. These f'_{ice} values
correspond to $P_{\lambda}(k \geq 1)_{\text{measured}}$ and can be used to infer the average INP concentration from Eq. (7). Because in the current
300 experiments the INP concentrations are known (i.e., 1.4×10^7 , 2.8×10^6 , and $1.4 \times 10^6\text{ mL}^{-1}$), these experimentally derived f'_{ice}
values can be compared to the expected f_{ice} values, corresponding to $P_{\lambda}(k \geq 1)_{\text{calculated}}$ values calculated from Eq. (7), yielding
values of 1.00 ± 0.01 , 0.66 ± 0.06 , and 0.41 ± 0.05 , respectively. These theoretical values are in good agreement (within
experimental uncertainty) with the measured values and thus confirm our approach and the inferred INP concentrations of
 1.2×10^7 , 2.5×10^6 , and $1.3 \times 10^6\text{ mL}^{-1}$ (see Supplementary Table S3) deviate by about 14%, 11% and 7% from the prepared
305 concentrations, which is very good given that INP concentrations can vary by orders of magnitude. For further validation that
the Poisson distribution is necessary for a proper evaluation in the above-mentioned concentration range, the cumulative
number of active ice-nucleating sites n_N per number of *P. syringae* bacteria was evaluated and discussed in the text describing
Supplementary Fig. S5.

3 Results and Discussion

310 3.1 Ice nucleation of *F. cylindrus*

3.1.1 Differential Scanning Calorimetry

As an initial experiment, the ice nucleation activity of *F. cylindrus* diatom cells was studied by differential scanning
calorimetry. For these measurements, an inverse emulsion of pure artificial seawater as a reference was compared with an
emulsion of artificial seawater containing 1×10^7 *F. cylindrus* cells per mL, see Fig. 4.



315

320

Figure 4: Comparison of DSC thermograms of water-in-oil emulsions containing pure artificial seawater and artificial seawater with *F. cylindrus* cells. **(a)** The endothermic melting-signals are almost identical for pure seawater and seawater containing diatoms. **(b)** Exothermic freezing signals for pure seawater and seawater containing diatoms. While the seawater emulsion shows only one freezing signal, the emulsion containing *F. cylindrus* shows the same signal but with a shoulder and smaller signals at higher temperature, indicative of diatom-induced heterogeneous ice nucleation.

First, the endothermic ice melting signals of the reference and the sample in Fig. 4a show almost the same signal, indicating that any colligative effect of the diatoms is negligible when compared to the amount of the dissolved ions in the artificial seawater. This similarity in the ice melting signals also implies no change in water activity of the artificial seawater upon the addition of the diatoms and, thus, no colligative effect on the homogeneous ice nucleation (freezing) signals is to be expected



- 325 The exothermic freezing signals for both emulsions are shown in Fig. 4b. For the seawater reference, one distinct nearly symmetrical freezing signal is revealed with a maximum at about $-44\text{ }^{\circ}\text{C}$ and an onset at about $-40\text{ }^{\circ}\text{C}$. In contrast, the *F. cylindrus* sample shows the same maximum, but in addition a second exothermic signal in the form of a shoulder at about $-42\text{ }^{\circ}\text{C}$, with an onset at a somewhat higher temperature of $-39\text{ }^{\circ}\text{C}$ when compared to the reference, and with small signals as high as $-34\text{ }^{\circ}\text{C}$.
- 330 The larger broad signal in both emulsion samples corresponds to the homogeneous ice nucleation temperature of artificial seawater. This signal is also observed in the *F. cylindrus* sample because many of the emulsion droplets in that sample do not contain diatoms. The exothermic shoulder of the signal, which is not present in the reference, is most likely due to the freezing of droplets containing a diatom cell or fragment, and the shift of the onset to higher temperature is a first indication for the heterogeneous ice nucleation activity of the diatoms.
- 335 Because of the fact that the diatoms are of similar size as the emulsion droplets and the potential of mechanical disruption of diatom cells during the fast stirring of the disperser during emulsion preparation, these emulsion experiments appear to us as not suitable for a quantitative analysis of the ice nucleation activity of *F. cylindrus*. Thus, we employed non-invasive methods in the experiments described below.

3.1.2 Droplet Microfluidics

- 340 First, we investigated the ice-nucleating properties of samples containing *F. cylindrus* diatoms at different concentration suspended in artificial seawater. For this purpose, we made use of the droplet microfluidic devices described in Sect. 2.3.2 above. The results of these experiments are presented in Fig. 5a, which shows, as a function of temperature, the frozen fraction of droplets f_{ice} , commonly defined as the cumulative number of droplets frozen when cooled to a certain temperature relative to the total number of droplets (Murray et al., 2012). Thus, f_{ice} is practically independent of the total number of droplets
- 345 investigated in a particular experiment. In our case, the number of droplets varied between 45 and 70 droplets per single measurement, and typically three single measurements per sample were performed. Figure 5a shows that the freezing temperatures of all *F. cylindrus* samples (coloured symbols) are higher than that of the artificial seawater reference sample (grey symbols), hence supporting the observations from the DSC experiments above that the *F. cylindrus* diatoms promote ice nucleation. To compare the different samples, we use the T_{50} temperature, which is defined as that temperature at which half
- 350 of the observed droplets are frozen, i.e. $f_{\text{ice}} = 0.5$. For the artificial seawater, we measured a T_{50} of $-40.1\text{ }^{\circ}\text{C}$, and T_{50} of the *F. cylindrus* suspensions is shifted to higher temperature by about $2.8\text{ }^{\circ}\text{C}$ to $7.2\text{ }^{\circ}\text{C}$ with increasing diatom concentration. Detailed information on the increase in T_{50} of the different concentrations is given in the Supplemental Information Table S4. This significant concentration dependence of the T_{50} shift reveals that not all diatoms nucleate ice at exactly the same temperature and implies a distribution of the ice nucleation efficiency as has been observed previously also for other ice
- 355 nucleators (Herbert et al., 2014; Budke and Koop, 2015).

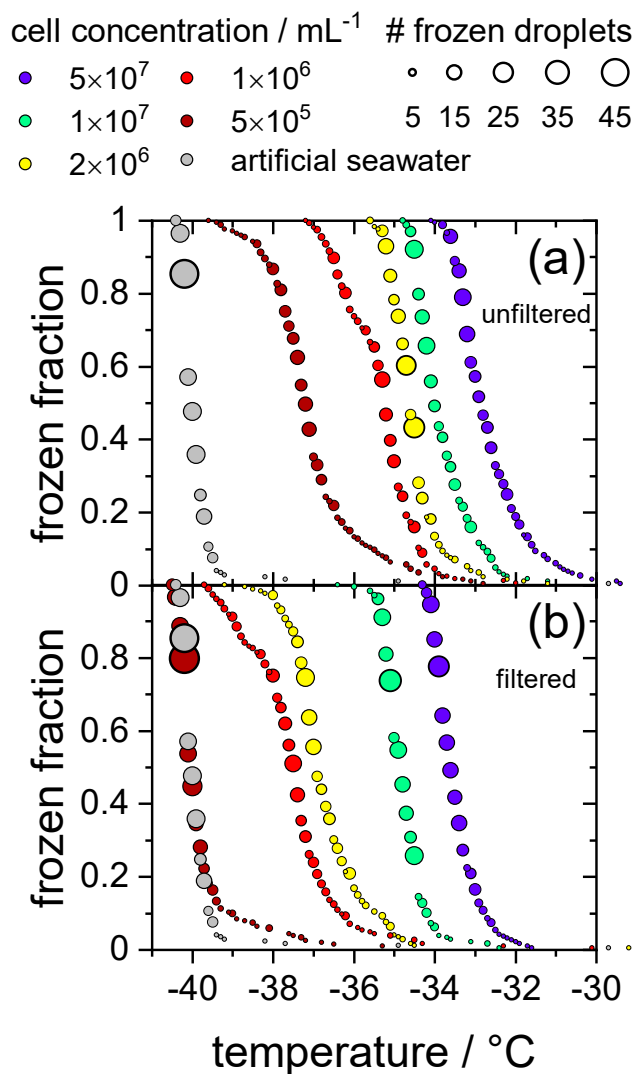


Figure 5: Cumulative fraction of frozen droplets as a function of temperature for different *F. cylindrus* concentrations (coloured circles) and pure artificial seawater (grey circles) as a reference. The size of the circles indicates the number of droplets frozen within the same temperature interval (0.1 °C). Each dataset combines three individual measurements containing each between 45 and 70 droplets. **(a):** Frozen fraction curves for the five *F. cylindrus* samples, containing mostly whole diatoms and, probably, some fragments. **(b):** Freezing temperatures of the same samples shown in panel (a), but after filtration with a pore size of 0.22 μm. These samples, thus, contain no whole cells but fragments as well as proteins and other soluble components. Note that the concentrations refer to the diatom concentrations before filtration. The seawater reference (grey circles) is the same in both panels.

This fact can be visualized better by plotting the cumulative number n_N of ice nucleating sites per number of *F. cylindrus* diatoms, defined in Eq. (S2), as a function of freezing temperature, see Fig. 6. This n_N value is independent of the concentration of investigated INP and of the size of the investigated droplets, but can be measured for a wide range of temperatures using different concentrations, and allows for the comparison with results from other experimental techniques (see discussion below). Figure 6 reveals that at -30.0 °C ~0.1 % of the *F. cylindrus* diatoms promote ice nucleation, which increases to ~1 % at -32.0



°C and ~10 % at -33.5 °C. Between about -35.0 °C and -36.5 °C all diatoms trigger the nucleation of ice, i.e. $n_N = 1$. By
370 definition, n_N values larger than one should not be possible, because it would imply that one diatom can induce the freezing
of more than one droplet, which is unreasonable. The highest n_N values occur at the lowest diatom concentrations and,
therefore, we must consider the Poisson range defined above, i.e. whether or not each droplet does indeed contain a diatom
cell. Following the treatise in Sect. 2.3.3 using Eq. (7), we indicate in Fig. 6 all droplets that contain at least one diatom as
filled circles, while all droplets that do not contain any *F. cylindrus* are displayed as open circles. This analysis reveals a
375 relatively sharp transition between filled and unfilled circles at n_N values of about one ice nucleating active site per diatom
cell. All droplets frozen at $n_N \geq 1$ (and lower temperatures) do not contain intact *F. cylindrus* diatoms. We suggest that their
freezing is induced by cell fragments or by INPs released by the *F. cylindrus* diatoms, e.g. soluble species from the EPS such
as proteins. A similar behaviour has been observed previously for birch pollen that release about 10^4 ice nucleators per pollen
particle, which turned out to be ice-nucleating macromolecules (Pummer et al., 2012; Augustin et al., 2013; Pummer et al.,
380 2015; Dreischmeier et al., 2017).

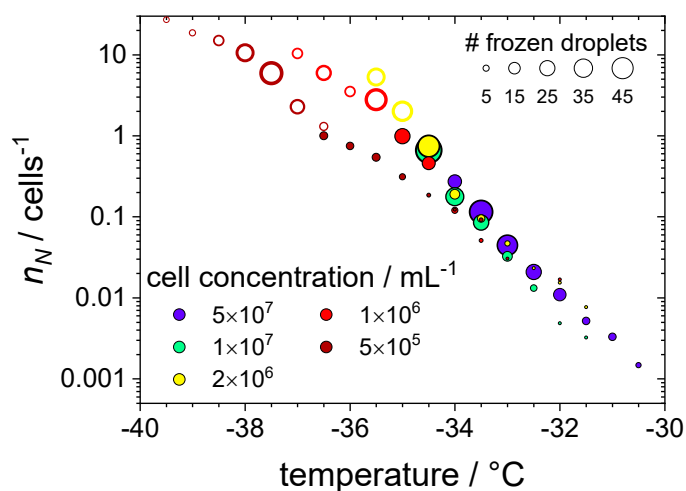


Figure 6: Cumulative number of ice nucleating sites n_N per number of *F. cylindrus* diatom cells as a function of temperature, obtained from
the data shown in Fig. 5a with the help of Eq. (S2). The original data were binned into intervals of 0.5 °C. The size of the circle symbols
385 indicates the absolute number of droplets frozen in a particular bin, and the cell concentrations per mL are indicated by colour. The filled
circles represent the droplets that contain whole *F. cylindrus* cells, while Poisson statistics suggest that the open circles should not contain
any whole diatoms but probably some cell fragments, see text.

To verify the above interpretation, we performed experiments in which the samples from the measurements shown in Fig. 5a
and Fig. 6 were filtered with a pore size of 0.22 μm . This procedure should remove intact whole diatoms, whose size is about
390 4.5 to 74 μm for the apical axis and 2.4 to 4 μm for the transapical axis (Lundholm and Hasle, 2008; Cefarelli et al., 2010). In
Fig. 5b, the cumulative fraction of frozen droplets of these filtered samples is shown. The symbol colours represent the same
suspensions as shown in Fig. 5a, but this time filtered, and the artificial seawater reference data identical to that in panel (a).
All frozen fraction curves are shifted to lower temperatures when compared to the unfiltered samples, suggesting a significant



395 but not entire removal of INPs. Only the filtrate of the suspension with the smallest concentrations reveals a T_{50} that is the same as the seawater reference (-40.1 °C), suggesting that this sample does not contain any significant concentration of INPs after filtration. All other filtrated suspensions show T_{50} values that are higher by between 2.6 °C and 6.4 °C relative to the seawater. For further information on the T_{50} shifts, see Supplementary Table S4. Together these results imply that indeed either fragments of *F. cylindrus* or molecules released by the diatoms can nucleate ice, but with a significantly reduced efficiency than intact diatoms. Moreover, these results can also explain the observations in Fig. 6 of ice nucleation of droplets at $n_N \geq 1$
400 that should not contain any diatoms. Below, we present further experiments to investigate the nature of the ice-nucleating particles.

3.3 Ice nucleation of resuspended *F. cylindrus* cells

In the following experiments, we tried to separate diatoms from their fragments or any released INPs. For this purpose, the sample suspension of *F. cylindrus* with a concentration of 10^7 cells per mL, which was shown already in Fig. 5 above, was
405 analysed further, and the results are presented in Fig. 7. The green data points are those of the unfiltered sample and is identical to that shown in Fig. 5a, and the magenta data points is identical to the filtered solution already presented in Fig. 5b (there as green data points). This sample suspension should contain only INPs smaller than 0.22 μm . Next, most (but not all) of the diatom cells and fragments contained in the filter cake of that filtration procedure were resuspended in artificial seawater. Thus, the concentration of the resuspended cells is probably significantly smaller than 10^7 cells per mL. The frozen fraction of
410 that sample is shown as the orange data points in Fig. 7 and shows the same onset ice nucleation temperature of about -32.5 °C as the original unfiltered suspension (green), however, the curve is much broader suggesting that it indeed contain much less of the most active ice nucleators. In order to verify that all fragments smaller than 0.22 μm had been leached out during the first filtration step, this resuspended filter cake sample was filtered again with a 0.22 μm filter. The results of this procedure on the freezing behaviour is shown as the blue circles in Fig. 7. These frozen fraction data are practically identical to that of
415 the artificial seawater, strongly suggesting that indeed filtration of the pure whole cells had been successful and hardly any fragments smaller than 0.22 μm are left in the filtrate. This analysis also implies that the ice nucleation of the unfiltered suspension is due to whole cells as well as cell fragments, but not due to ice-nucleating molecules released from the diatoms. The T_{50} shift upon filtration of about 1.5 °C is similar in magnitude to the effect of reducing the concentration of the unfiltered diatoms from 5×10^7 cells per mL to 1×10^7 cells per mL, i.e. by a factor of 5. This similarity may indicate that fragments make
420 up about 10-20% of the INPs in the unfiltered samples, which is in agreement with the fact that some ice nucleation is observed for values of $n_N \geq 1$, see Fig. 6.

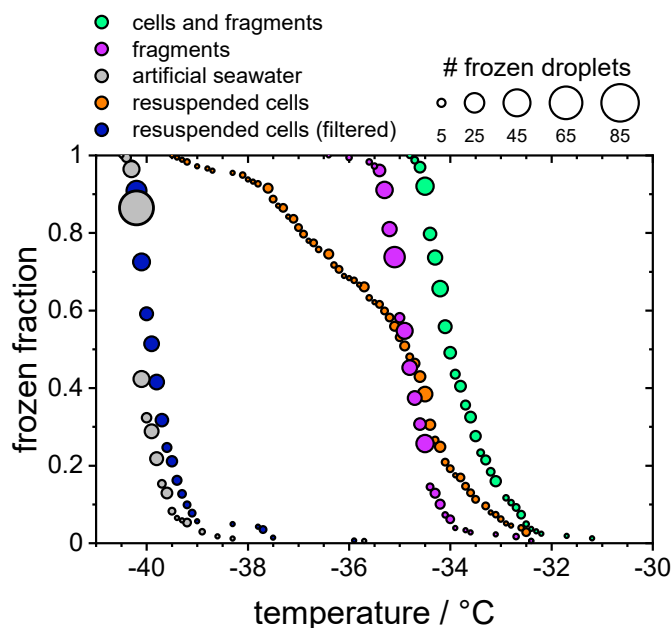


Figure 7: The frozen fraction of a sample with 10^7 *F. cylindrus* diatoms per mL after different treatments. The symbol size indicates the total number of droplets frozen at that temperature. The green coloured data are the untreated sample and are the same as those in Fig. 5a. The magenta data are the filtered sample that should just contain fragments of the diatoms. It is the same data as the green data in Fig. 5b. The grey data points show the freezing of the artificial seawater for reference (also replotted from Fig. 5). The orange data show the freezing of the diatoms that were resuspended from the filter into artificial seawater. Its concentration is likely smaller than 10^7 cells per mL, because not all cells could be resuspended. The blue data points represent the freezing of the droplets consisting of the resuspended cell suspension after renewed filtration: it should not contain any diatoms or fragments.

430 3.4 Ice nucleation of spent medium and of purified *fc*IBP11

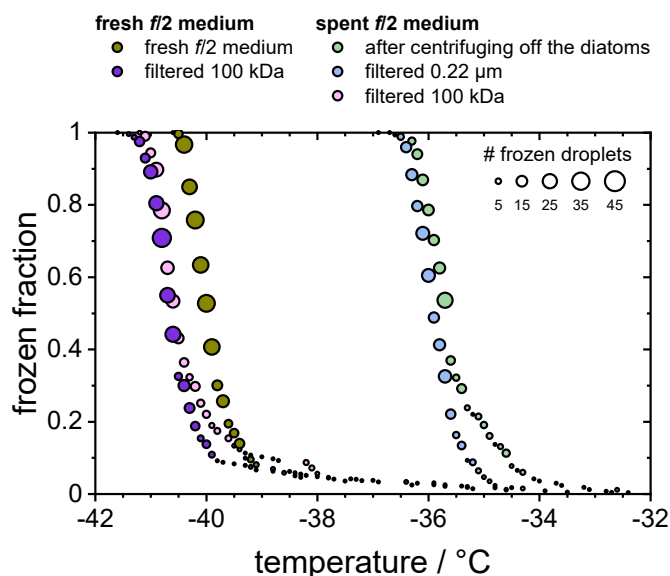
We also investigated the spent *f*2 medium (Guillard and Ryther, 1962), i.e., the medium in which the *F. cylindrus* diatoms were cultivated before they were separated by centrifugation to investigate their ice nucleating effects. Separation of the diatoms from the spent *f*2 medium by centrifugation is not perfect and, hence, smaller fragments as well as soluble macromolecules such as proteins may remain in the spent medium. These may be potential ice nucleators, as it has been shown previously that even smaller ice-binding antifreeze proteins can act as ice nucleators at lower temperatures (Eickhoff et al., 2019).

In Fig. 8 we compare the frozen fraction curve for the spent *f*2 medium (light green circles) with that of a freshly prepared *f*2 medium, which never had been in contact to any *F. cylindrus* diatoms (olive circles). Clearly, the spent medium, even after centrifuging off the diatoms, shows significant ice nucleation with a T_{50} of about -35.7 °C, while the T_{50} of the fresh medium is much lower at -40.0 °C. In additional experiments, the spent medium has been filtered in two further steps, first by using a 0.22 μm syringe filter (light blue circles) and then by using a 100 kDa centrifugation filter (pink circles). For comparison the fresh medium has been also filtered with a 100 kDa centrifugation filter (purple circles). Obviously, filtration of the spent



445

medium with a 0.22 μm filter shows hardly any effect on ice nucleation as its T_{50} is shifted to $-36.0\text{ }^\circ\text{C}$, which is the same as the unfiltered sample within the temperature uncertainty of our setup of $\pm 0.3\text{ }^\circ\text{C}$.



450

Figure 8: Frozen fraction of differently treated *f/2* nutria media as a function of temperature. The olive and purple circles belong to a fresh *f/2* medium that is untreated (olive) or had been filtered using a 100 kDa filter (purple). The green, blue and pink circles belong to the untreated, 0.22 μm filtered and 100 kDa filtered spent medium, in which the *F. cylindrus* diatoms had grown before they were centrifuged and separated from the medium.

455

In contrast, filtration with a 100 kDa filter resulted in a strongly reduced ice nucleation with a T_{50} value of $-40.6\text{ }^\circ\text{C}$, which is the same as that of the filtrated fresh medium of $-40.7\text{ }^\circ\text{C}$, suggesting that the 100 kDa filter removed all remaining ice nucleators present in the spent medium. This observation suggests that any macromolecules smaller than 100 kDa that were present in the spent medium are not ice nucleation active, because otherwise they had passed the filter and led to an increased

460

T_{50} when compared to the fresh medium. The ice-binding proteins present in and/or released from *F. cylindrus* are similar in size to the well characterized *fcIBP11*, which is about 26 kDa (Bayer-Giraldi et al., 2011). Thus, ice-binding proteins released by the *F. cylindrus* into the spent medium should have passed the filter and could have induced ice nucleation, if they had significant ice nucleation activity. However, the results shown in Fig. 8 do not reveal any ice nucleation activity and, thus, can be interpreted as follows. Either, any proteins remaining in the filtrate do not promote ice nucleation or, alternatively, *F.*

465

cylindrus does not release any proteins into the spent medium. In order to shed further light on the ice-nucleating ability of ice-binding proteins from *F. cylindrus*, we studied purified *fcIBP11* samples in additional experiments. We studied ice nucleation of two *fcIBP11* solutions of different concentration as well as that of the pure Tris-HCl buffer for comparison. The results are presented in Fig. 9. The two *fcIBP11* samples with concentrations of 0.1 mM (dark blue circles) and 0.01 mM (light blue circles) reveal T_{50} values of $-39.8\text{ }^\circ\text{C}$ and $-39.4\text{ }^\circ\text{C}$, which are equal to the $T_{50} = -39.7\text{ }^\circ\text{C}$ of the buffer reference (black circles) within experimental temperature uncertainty ($\pm 0.3\text{ }^\circ\text{C}$). Thus, no significant shift in the freezing temperature is



observed, and even when considering the increased ice nucleation temperature of the *fcIBP11* at frozen fractions below about 25% it appears that *fcIBP11* is not an efficient ice nucleator with relevance for atmospheric or biospheric processes, owing to its unnaturally high concentration in the droplet samples investigated here. These observations are in a good agreement with recent theoretical studies, which suggest that moderate IBPs show no nucleation of ice perpendicular to the basal and prismatic ice planes (Cui et al., 2022). And indeed, these basal and prismatic planes are exactly those planes, at which the moderate *fcIBP11* binds to ice (Kondo et al., 2018).

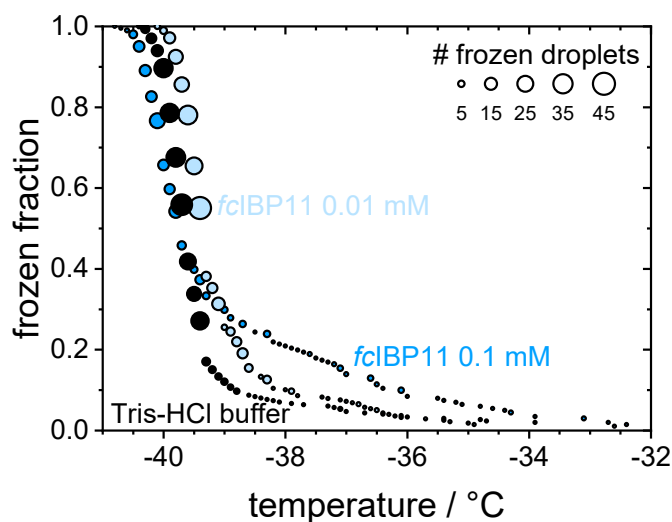


Figure 9: Cumulative frozen fractions as a function of temperature of droplets containing *fcIBP11* solutions with concentrations of 0.1 mmol per L (dark blue) and 0.01 mmol per L (light blue). The black circles show the freezing of the Tris-HCl buffer for reference. The circle area indicates the number of droplets frozen at a particular temperature.

Overall, the results show that *F. cylindrus* diatom cells as well as cell fragments suspended in seawater can induce heterogeneous ice nucleation, while ice-binding proteins produced by *F. cylindrus* such as *fcIBP11* have negligible ice nucleation activity.

480 4 Discussion and Implications

Here, we put the results obtained above in the context of previous ice nucleation studies on diatoms. Triggered by the pioneering initial laboratory studies of marine diatom-induced ice nucleation (Alpert et al., 2011; Knopf et al., 2011) modelling studies have shown that in some regions of the atmosphere marine diatoms may indeed contribute to atmospheric INP (Burrows et al., 2013; Ickes et al., 2020). In order to use laboratory ice nucleation data in such models, the data have to be evaluated and parameterized appropriately. For example, a direct comparison of T_{50} or f_{ice} originating from different laboratory studies on different types of INPs it not meaningful, as different sample volumes, INP concentrations, buffer concentrations, etc. may have been used. Therefore, it is preferable to compare the cumulative number of ice nucleating active sites per mass, surface



area or number of the INPs. Here, we make a comparison based on total INP mass, using the following definition of the cumulative number of ice nucleating active sites per mass n_{m_total} (Murray et al., 2012; Hiranuma et al., 2015; Hiranuma et al., 2019; Xi et al., 2021).

$$n_{m_total} = \frac{-\ln(1-f_{ice})}{c_{m_total} \cdot V} \quad (8)$$

Here, V is the volume of an individual droplet in the experiment and c_{m_total} is the total mass of biological material per droplet. For the *F. cylindrus* samples investigated here, we used the total carbon mass per *F. cylindrus* cell from the literature (Kang and Fryxell, 1992) and used elementary analysis to obtain the carbon content of our samples resulting in a value of 39.32 %. Using these values and our experimental data in Eq. (8), we have calculated the ice nucleating active sites n_{m_total} of the *F. cylindrus* diatoms, see the blue circles in Fig. 10. (We have fitted this data set and provide a corresponding parameterization, see Supplementary Fig. S6 and Eq. (S3).) Also shown in Fig. 10 are n_{m_total} data of other the sea ice diatoms *Melosira arctica* (blue squares) and *Nitzschia stellata* (blue triangles) and of the temperate diatom *Skeletonema marinoi* (open red circles) from previous studies (Ickes et al., 2020; Xi et al., 2021).

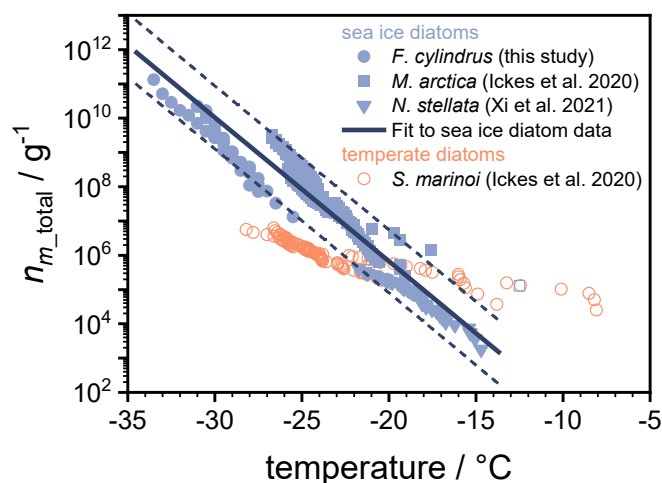


Figure 10: Experimental data of n_{m_total} , i.e. the number of ice active sites per total mass of *F. cylindrus* diatom cells (blue circles) and other sea ice diatoms (blue squares and triangles) from previous studies, as well as n_{m_total} data for one temperate diatom species (open red circles) (Ickes et al., 2020; Xi et al., 2021). The solid line represents a fit of the n_{m_total} values for the three sea ice diatom species (see Eq. (9)), while the dashed lines indicate the 2σ upper and lower prediction bands of this fit. All temperatures were corrected for the freezing point depressions of different buffers and solutes, so that they represent the ice nucleation induced by the diatoms in pure water.

The n_{m_total} values for *N. stellata* were provided by the authors (Xi et al., 2021). For *M. arctica* and the *S. marinoi*, we calculated n_{m_total} from the total number of cells given in the original work and provided by the authors (Ickes et al., 2020), and assume cell volumes of $653 \mu\text{m}^3$ and $125 \mu\text{m}^3$ and a cell density of 1 mg mL^{-1} (Olenina et al., 2006; Xi et al., 2021). In order to allow a direct comparison of ice nucleation of the different diatoms, which were studied in different types of aqueous



solution, all the ice nucleation temperatures shown in Fig. 10 have been corrected for the colligative solute effect and represent diatom ice nucleation in pure water.

The comparison in Fig. 10 reveals that the curves of the three sea ice diatoms complement one another as n_{m_total} values of
515 different magnitude have been obtained over different temperature ranges. Interestingly, while there are some offsets between the different data sets, their slopes are quite similar. In contrast, the slope of the n_{m_total} data of the temperate diatom is significantly smaller. The observed similarities of the sea ice diatom data sets suggest a more generalized description of their behaviour in models. For this purpose, we fitted these data sets to provide a parametrization of n_{m_total} as a function of temperature. The three different data sets consist of different numbers of data points, which was taken into account in order to
520 give each data set the same statistical weight. We further note that one strongly deviating data point from the *M. arctica* data set (indicated as an open square in Fig. 10) was excluded from the fitting procedure. The resulting parameterization is given as:

$$\log_{10}(n_{m_total} \text{ g}^{-1}) = -0.420053 \text{ } ^\circ\text{C}^{-1} \cdot T - 2.57818 \quad (9)$$

525

where T is temperature to be entered in units of $^\circ\text{C}$. For numerical code verification, Eq. (9) should result in a value for n_{m_total} of $6.7 \times 10^5 \text{ g}^{-1}$ at a temperature of $-20.0 \text{ } ^\circ\text{C}$. This parametrization is valid over the temperature range between $-13.7 \text{ } ^\circ\text{C}$ to $-34.5 \text{ } ^\circ\text{C}$ (i.e., 259.45 to 238.65 K). The parameterization is shown as the thick solid line in Fig. 10, and the upper and lower 2σ prediction bands are given as dashed lines. In summary, Fig. 10 shows that the parameterization line and its prediction bands
530 are an appropriate representation of the ice nucleation activity of three types of sea ice diatoms suitable for use in atmospheric or biogeosciences model applications.

5 Conclusions

F. cylindrus diatoms can induce heterogeneous ice nucleation in artificial seawater by as much as 7.2°C higher than pure seawater for the highest diatom concentration investigated, (5×10^7 cells per mL). We also observed an ice nucleating effect of
535 fragments smaller than $0.22 \text{ } \mu\text{m}$, in agreement with previous observations of the relevance of nanoscale biological fragments for ice nucleation in clouds (O'Sullivan et al., 2015; Wilson et al., 2015; Irish et al., 2017; Irish et al., 2019). We observed a common behaviour of the cumulative number of ice nucleating active sites per mass of diatom among three different types of sea ice diatoms. This similarity may originate from a similar biological function of the ice nucleation ability in seas-ice diatoms, and a corresponding parameterization developed thereof may simplify the representation of their properties in atmospheric
540 biogeoscientific models.



Data availability

The experimental data presented in this paper will be made freely available on a repository server of Bielefeld University upon final acceptance of the manuscript.

Author contribution

545 LE and TK designed the study. MBG provided the protein samples, LE performed the calibration and both the DSC and the microfluidic ice nucleation experiments, NR prepared the microfluidic devices. LE did the data analysis and the Poisson statistics calculations with input from TK. LE and TK prepared the figures, LE, TK and MBG wrote the manuscript with input from YR and NR. All authors contributed to the discussion of the data and text, and approved the final version of the manuscript.

550 Competing interests

The authors declare that they have no conflict of interest.

Acknowledgements

We thank Arika Allhusen and Klaus Valentin for providing the original *F. cylindrus* samples, and Luisa Ickes, Yu Xi and Allan Bertram for provision of original data sets on diatom ice nucleation and for helpful comments. We acknowledge support
555 for the publication costs by the Open Access Publication Fund of Bielefeld University and the Deutsche Forschungsgemeinschaft (DFG).

References

- Ackley, S. F. and Sullivan, C. W.: Physical controls on the development and characteristics of Antarctic sea ice biological communities— a review and synthesis, *Deep Sea Research Part I: Oceanographic Research Papers*, 41, 1583–1604,
560 doi:10.1016/0967-0637(94)90062-0, 1994.
- Alpert, P. A., Aller, J. Y., and Knopf, D. A.: Ice nucleation from aqueous NaCl droplets with and without marine diatoms, *Atmos. Chem. Phys.*, 11, 5539–5555, doi:10.5194/acp-11-5539-2011, 2011.
- Aslam, S. N., Cresswell-Maynard, T., Thomas, D. N., and Underwood, G. J. C.: Production and Characterization of the Intra- and Extracellular Carbohydrates and Polymeric Substances (EPS) of Three Sea-Ice Diatom Species, and Evidence for a
565 Cryoprotective Role for EPS, *Journal of phycology*, 48, 1494–1509, doi:10.1111/jpy.12004, 2012a.



- Aslam, S. N., Strauss, J., Thomas, D. N., Mock, T., and Underwood, G. J. C.: Identifying metabolic pathways for production of extracellular polymeric substances by the diatom *Fragilariopsis cylindrus* inhabiting sea ice, *The ISME journal*, 12, 1237–1251, doi:10.1038/s41396-017-0039-z, 2018.
- Aslam, S. N., Underwood, G. J. C., Kaartokallio, H., Norman, L., Autio, R., Fischer, M., Kuosa, H., Dieckmann, G. S., and
570 Thomas, D. N.: Dissolved extracellular polymeric substances (dEPS) dynamics and bacterial growth during sea ice formation in an ice tank study, *Polar Biol*, 35, 661–676, doi:10.1007/s00300-011-1112-0, 2012b.
- Augustin, S., Wex, H., Niedermeier, D., Pummer, B., Grothe, H., Hartmann, S., Tomsche, L., Clauss, T., Voigtländer, J., Ignatius, K., and Stratmann, F.: Immersion freezing of birch pollen washing water, *Atmos. Chem. Phys.*, 13, 10989–11003, doi:10.5194/acp-13-10989-2013, 2013.
- 575 Bar Dolev, M., Braslavsky, I., and Davies, P. L.: Ice-Binding Proteins and Their Function, *Annual review of biochemistry*, 85, 515–542, doi:10.1146/annurev-biochem-060815-014546, 2016.
- Bartsch, A.: Sea Ice Algae of the Weddell Sea (Antarctica): Species Composition, Biomass, and Ecophysiology of Selected Species, *Ber. Polarforsch.*, 63, 1989.
- Bayer-Giraldi, M., Sazaki, G., Nagashima, K., Kipfstuhl, S., Vorontsov, D. A., and Furukawa, Y.: Growth suppression of ice
580 crystal basal face in the presence of a moderate ice-binding protein does not confer hyperactivity, *Proceedings of the National Academy of Sciences of the United States of America*, 115, 7479–7484, doi:10.1073/pnas.1807461115, 2018.
- Bayer-Giraldi, M., Uhlig, C., John, U., Mock, T., and Valentin, K.: Antifreeze proteins in polar sea ice diatoms: diversity and gene expression in the genus *Fragilariopsis*, *Environmental microbiology*, 12, 1041–1052, doi:10.1111/j.1462-2920.2009.02149.x, 2010.
- 585 Bayer-Giraldi, M., Weikusat, I., Besir, H., and Dieckmann, G.: Characterization of an antifreeze protein from the polar diatom *Fragilariopsis cylindrus* and its relevance in sea ice, *Cryobiology*, 63, 210–219, doi:10.1016/j.cryobiol.2011.08.006, 2011.
- Budke, C. and Koop, T.: BINARY: an optical freezing array for assessing temperature and time dependence of heterogeneous ice nucleation, *Atmos. Meas. Tech.*, 8, 689–703, doi:10.5194/amt-8-689-2015, 2015.
- Burrows, S. M., Hoose, C., Pöschl, U., and Lawrence, M. G.: Ice nuclei in marine air: biogenic particles or dust?, *Atmos.*
590 *Chem. Phys.*, 13, 245–267, doi:10.5194/acp-13-245-2013, 2013.
- Cefarelli, A. O., Ferrario, M. E., Almandoz, G. O., Atencio, A. G., Akselman, R., and Vernet, M.: Diversity of the diatom genus *Fragilariopsis* in the Argentine Sea and Antarctic waters: morphology, distribution and abundance, *Polar Biol*, 33, 1463–1484, doi:10.1007/s00300-010-0794-z, 2010.
- Collins, D. J., Neild, A., deMello, A., Liu, A.-Q., and Ai, Y.: The Poisson distribution and beyond: methods for microfluidic
595 droplet production and single cell encapsulation, *Lab on a chip*, 15, 3439–3459, doi:10.1039/c5lc00614g, 2015.
- Creamean, J. M., Cenicerros, J. E., Newman, L., Pace, A. D., Hill, T. C. J., DeMott, P. J., and Rhodes, M. E.: Evaluating the potential for Haloarchaea to serve as ice nucleating particles, *Biogeosciences*, 18, 3751–3762, doi:10.5194/bg-18-3751-2021, 2021.



- Creamean, J. M., Hill, T. C. J., DeMott, P. J., Uetake, J., Kreidenweis, S., and Douglas, T. A.: Thawing permafrost: an
600 overlooked source of seeds for Arctic cloud formation, *Environ. Res. Lett.*, 15, 84022, doi:10.1088/1748-9326/ab87d3,
2020.
- Cui, S., Zhang, W., Shao, X., and Cai, W.: Do Antifreeze Proteins Generally Possess the Potential to Promote Ice Growth?,
Phys. Chem. Chem. Phys., doi:10.1039/D1CP05431G, 2022.
- Davies, P. L.: Ice-binding proteins: a remarkable diversity of structures for stopping and starting ice growth, *Trends in*
605 *Biochemical Sciences*, 39, 548–555, doi:10.1016/j.tibs.2014.09.005, 2014.
- DeMott, P. J., Hill, T. C. J., McCluskey, C. S., Prather, K. A., Collins, D. B., Sullivan, R. C., Ruppel, M. J., Mason, R. H.,
Irish, V. E., Lee, T., Hwang, C. Y., Rhee, T. S., Snider, J. R., McMeeking, G. R., Dhaniyala, S., Lewis, E. R., Wentzell,
J. J. B., Abbatt, J., Lee, C., Sultana, C. M., Ault, A. P., Axson, J. L., Diaz Martinez, M., Venero, I., Santos-Figueroa, G.,
Stokes, M. D., Deane, G. B., Mayol-Bracero, O. L., Grassian, V. H., Bertram, T. H., Bertram, A. K., Moffett, B. F., and
610 Franc, G. D.: Sea spray aerosol as a unique source of ice nucleating particles, *Proceedings of the National Academy of*
Sciences of the United States of America, 113, 5797–5803, doi:10.1073/pnas.1514034112, 2016.
- DeMott, P. J., Möhler, O., Cziczo, D. J., Hiranuma, N., Petters, M. D., Petters, S. S., Belosi, F., Bingemer, H. G., Brooks, S.
D., Budke, C., Burkert-Kohn, M., Collier, K. N., Danielczok, A., Eppers, O., Felgitsch, L., Garimella, S., Grothe, H.,
Herenz, P., Hill, T. C. J., Höhler, K., Kanji, Z. A., Kiselev, A., Koop, T., Kristensen, T. B., Krüger, K., Kulkarni, G.,
615 Levin, E. J. T., Murray, B. J., Nicosia, A., O'Sullivan, D., Peckhaus, A., Polen, M. J., Price, H. C., Reicher, N., Rothenberg,
D. A., Rudich, Y., Santachiara, G., Schiebel, T., Schrod, J., Seifried, T. M., Stratmann, F., Sullivan, R. C., Suski, K. J.,
Szakáll, M., Taylor, H. P., Ullrich, R., Vergara-Temprado, J., Wagner, R., Whale, T. F., Weber, D., Welti, A., Wilson, T.
W., Wolf, M. J., and Zenker, J.: The Fifth International Workshop on Ice Nucleation phase 2 (FIN-02): laboratory
intercomparison of ice nucleation measurements, *Atmos. Meas. Tech.*, 11, 6231–6257, doi:10.5194/amt-11-6231-2018,
620 2018.
- Dreichsmeier, K., Budke, C., Wiehemeier, L., Kottke, T., and Koop, T.: Boreal pollen contain ice-nucleating as well as ice-
binding 'antifreeze' polysaccharides, *Scientific reports*, 7, 41890, doi:10.1038/srep41890, 2017.
- Edd, J. F., Humphry, K. J., Irimia, D., Weitz, D. A., and Toner, M.: Nucleation and solidification in static arrays of
monodisperse drops, *Lab on a chip*, 9, 1859–1865, doi:10.1039/b821785h, 2009.
- 625 Eicken, H.: The role of sea ice in structuring Antarctic ecosystems, *Polar Biol*, 12, doi:10.1007/BF00239960, 1992.
- Eickhoff, L., Dreischmeier, K., Zipori, A., Sirovinskaya, V., Adar, C., Reicher, N., Braslavsky, I., Rudich, Y., and Koop, T.:
Contrasting Behavior of Antifreeze Proteins: Ice Growth Inhibitors and Ice Nucleation Promoters, *The journal of physical*
chemistry letters, 10, 966–972, doi:10.1021/acs.jpcclett.8b03719, 2019.
- Garrison, D. and Buck, K.: The biota of Antarctic pack ice in the Weddell sea and Antarctic Peninsula regions, *Polar Biol*, 10,
630 doi:10.1007/BF00238497, 1989.



- Gersonde, R. and Zielinski, U.: The reconstruction of late Quaternary Antarctic sea-ice distribution—the use of diatoms as a proxy for sea-ice, *Palaeogeography, Palaeoclimatology, Palaeoecology*, 162, 263–286, doi:10.1016/S0031-0182(00)00131-0, 2000.
- Govindarajan, A. G. and Lindow, S. E.: Size of Bacterial Ice-Nucleation Sites Measured in situ by Radiation Inactivation Analysis, *Proceedings of the National Academy of Sciences of the United States of America*, 85, 1334–1338, 1988.
- 635 Guillard, R. R. L. and Ryther, J. H.: Studies of marine planktonic diatoms: I. *Cyclotella nana* hustedt, and *Detonula convervacea* (cleve) gran, *Can. J. Microbiol.*, 8, 229–239, doi:10.1139/m62-029, 1962.
- Günther, S. and Dieckmann, G. S.: Vertical zonation and community transition of sea-ice diatoms in fast ice and platelet layer, Weddell Sea, Antarctica, *Ann. Glaciol.*, 33, 287–296, doi:10.3189/172756401781818590, 2001.
- 640 Gute, E. and Abbatt, J. P.: Ice nucleating behavior of different tree pollen in the immersion mode, *Atmospheric Environment*, 231, 117488, doi:10.1016/j.atmosenv.2020.117488, 2020.
- Hartmann, M., Gong, X., Kecorius, S., van Pinxteren, M., Vogl, T., Welti, A., Wex, H., Zeppenfeld, S., Herrmann, H., Wiedensohler, A., and Stratmann, F.: Terrestrial or marine – indications towards the origin of ice-nucleating particles during melt season in the European Arctic up to 83.7° N, *Atmos. Chem. Phys.*, 21, 11613–11636, doi:10.5194/acp-21-11613-2021, 2021.
- 645 Herbert, R. J., Murray, B. J., Whale, T. F., Dobbie, S. J., and Atkinson, J. D.: Representing time-dependent freezing behaviour in immersion mode ice nucleation, *Atmos. Chem. Phys.*, 14, 8501–8520, doi:10.5194/acp-14-8501-2014, 2014.
- Hiranuma, N., Adachi, K., Bell, D. M., Belosi, F., Beydoun, H., Bhaduri, B., Bingemer, H., Budke, C., Clemen, H.-C., Conen, F., Cory, K. M., Curtius, J., DeMott, P. J., Eppers, O., Grawe, S., Hartmann, S., Hoffmann, N., Höhler, K., Jantsch, E., Kiselev, A., Koop, T., Kulkarni, G., Mayer, A., Murakami, M., Murray, B. J., Nicosia, A., Petters, M. D., Piazza, M., Polen, M., Reicher, N., Rudich, Y., Saito, A., Santachiara, G., Schiebel, T., Schill, G. P., Schneider, J., Segev, L., Stopelli, E., Sullivan, R. C., Suski, K., Szakáll, M., Tajiri, T., Taylor, H., Tobo, Y., Ullrich, R., Weber, D., Wex, H., Whale, T. F., Whiteside, C. L., Yamashita, K., Zelenyuk, A., and Möhler, O.: A comprehensive characterization of ice nucleation by three different types of cellulose particles immersed in water, *Atmos. Chem. Phys.*, 19, 4823–4849, doi:10.5194/acp-19-4823-2019, 2019.
- 655 Hiranuma, N., Augustin-Bauditz, S., Bingemer, H., Budke, C., Curtius, J., Danielczok, A., Diehl, K., Dreischmeier, K., Ebert, M., Frank, F., Hoffmann, N., Kandler, K., Kiselev, A., Koop, T., Leisner, T., Möhler, O., Nillius, B., Peckhaus, A., Rose, D., Weinbruch, S., Wex, H., Boose, Y., DeMott, P. J., Hader, J. D., Hill, T. C. J., Kanji, Z. A., Kulkarni, G., Levin, E. J. T., McCluskey, C. S., Murakami, M., Murray, B. J., Niedermeier, D., Petters, M. D., O'Sullivan, D., Saito, A., Schill, G. P., Tajiri, T., Tolbert, M. A., Welti, A., Whale, T. F., Wright, T. P., and Yamashita, K.: A comprehensive laboratory study on the immersion freezing behavior of illite NX particles: a comparison of 17 ice nucleation measurement techniques, *Atmos. Chem. Phys.*, 15, 2489–2518, doi:10.5194/acp-15-2489-2015, 2015.
- 660



- Hudait, A., Qiu, Y., Odendahl, N., and Molinero, V.: Hydrogen-Bonding and Hydrophobic Groups Contribute Equally to the Binding of Hyperactive Antifreeze and Ice-Nucleating Proteins to Ice, *Journal of the American Chemical Society*, 141, 7887–7898, doi:10.1021/jacs.9b02248, 2019.
- Huebner, A., Srisa-Art, M., Holt, D., Abell, C., Hollfelder, F., deMello, A. J., and Edel, J. B.: Quantitative detection of protein expression in single cells using droplet microfluidics, *Chemical communications (Cambridge, England)*, 1218–1220, doi:10.1039/b618570c, 2007.
- Ickes, L., Porter, G. C. E., Wagner, R., Adams, M. P., Bierbauer, S., Bertram, A. K., Bilde, M., Christiansen, S., Ekman, A. M. L., Gorokhova, E., Höhler, K., Kiselev, A. A., Leck, C., Möhler, O., Murray, B. J., Schiebel, T., Ullrich, R., and Salter, M. E.: The ice-nucleating activity of Arctic sea surface microlayer samples and marine algal cultures, *Atmos. Chem. Phys.*, 20, 11089–11117, doi:10.5194/acp-20-11089-2020, 2020.
- Irish, V. E., Elizondo, P., Chen, J., Chou, C., Charette, J., Lizotte, M., Ladino, L. A., Wilson, T. W., Gosselin, M., Murray, B. J., Polishchuk, E., Abbatt, J. P. D., Miller, L. A., and Bertram, A. K.: Ice-nucleating particles in Canadian Arctic sea-surface microlayer and bulk seawater, *Atmos. Chem. Phys.*, 17, 10583–10595, doi:10.5194/acp-17-10583-2017, 2017.
- Irish, V. E., Hanna, S. J., Xi, Y., Boyer, M., Polishchuk, E., Ahmed, M., Chen, J., Abbatt, J. P. D., Gosselin, M., Chang, R., Miller, L. A., and Bertram, A. K.: Revisiting properties and concentrations of ice-nucleating particles in the sea surface microlayer and bulk seawater in the Canadian Arctic during summer, *Atmos. Chem. Phys.*, 19, 7775–7787, doi:10.5194/acp-19-7775-2019, 2019.
- Kang, S.-H. and Fryxell, G.: *Fragilariopsis cylindrus* (Grunow) Krieger: The most abundant diatom in water column assemblages of Antarctic marginal ice-edge zones, *Polar Biol*, 12, doi:10.1007/BF00236984, 1992.
- Knopf, D. A., Alpert, P. A., Wang, B., and Aller, J. Y.: Stimulation of ice nucleation by marine diatoms, *Nature Geosci*, 4, 88–90, doi:10.1038/ngeo1037, 2011.
- Kondo, H., Mochizuki, K., and Bayer-Giraldi, M.: Multiple binding modes of a moderate ice-binding protein from a polar microalga, *Physical chemistry chemical physics PCCP*, 20, 25295–25303, doi:10.1039/c8cp04727h, 2018.
- Koop, T.: Homogeneous Ice Nucleation in Water and Aqueous Solutions, *Zeitschrift für Physikalische Chemie*, 218, 1231–1258, doi:10.1524/zpch.218.11.1231.50812, 2004.
- Koop, T., Luo, B., Biermann, U. M., Crutzen, P. J., and Peter, T.: Freezing of HNO₃/H₂SO₄/H₂O Solutions at Stratospheric Temperatures: Nucleation Statistics and Experiments, *J. Phys. Chem. A*, 101, 1117–1133, doi:10.1021/jp9626531, 1997.
- Koop, T. and Murray, B. J.: A physically constrained classical description of the homogeneous nucleation of ice in water, *The Journal of chemical physics*, 145, 211915, doi:10.1063/1.4962355, 2016.
- Köster, S., Angilè, F. E., Duan, H., Agresti, J. J., Wintner, A., Schmitz, C., Rowat, A. C., Merten, C. A., Pisignano, D., Griffiths, A. D., and Weitz, D. A.: Drop-based microfluidic devices for encapsulation of single cells, *Lab on a chip*, 8, 1110–1115, doi:10.1039/b802941e, 2008.



- 695 Krembs, C. and Engel, A.: Abundance and variability of microorganisms and transparent exopolymer particles across the ice-water interface of melting first-year sea ice in the Laptev Sea (Arctic), *Marine Biology*, 138, 173–185, doi:10.1007/s002270000396, 2001.
- Kunert, A. T., Pöhlker, M. L., Tang, K., Krevert, C. S., Wieder, C., Speth, K. R., Hanson, L. E., Morris, C. E., Schmale III, D. G., Pöschl, U., and Fröhlich-Nowoisky, J.: Macromolecular fungal ice nuclei in *Fusarium*: effects of physical and chemical
700 processing, *Biogeosciences*, 16, 4647–4659, doi:10.5194/bg-16-4647-2019, 2019.
- Leck, C. and Bigg, E. K.: Biogenic particles in the surface microlayer and overlaying atmosphere in the central Arctic Ocean during summer, *Tellus B: Chemical and Physical Meteorology*, 57, 305–316, doi:10.3402/tellusb.v57i4.16546, 2005.
- Lizotte, M. P.: The Contributions of Sea Ice Algae to Antarctic Marine Primary Production, *Am Zool*, 41, 57–73, doi:10.1093/icb/41.1.57, 2001.
- 705 Lundholm, N. and Hasle, G. R.: Are *Fragilariopsis cylindrus* and *Fragilariopsis nana* bipolar diatoms? - Morphological and molecular analyses of two sympatric species, *Nova Hedwigia, Beiheft*, 133, 231–250, 2008.
- Mock, T., Otilar, R. P., Strauss, J., McMullan, M., Paajanen, P., Schmutz, J., Salamov, A., Sanges, R., Toseland, A., Ward, B. J., Allen, A. E., Dupont, C. L., Frickenhaus, S., Maumus, F., Veluchamy, A., Wu, T., Barry, K. W., Falciatore, A., Ferrante, M. I., Fortunato, A. E., Glöckner, G., Gruber, A., Hipkin, R., Janech, M. G., Kroth, P. G., Leese, F., Lindquist,
710 E. A., Lyon, B. R., Martin, J., Mayer, C., Parker, M., Quesneville, H., Raymond, J. A., Uhlig, C., Valas, R. E., Valentin, K. U., Worden, A. Z., Armbrust, E. V., Clark, M. D., Bowler, C., Green, B. R., Moulton, V., van Oosterhout, C., and Grigoriev, I. V.: Evolutionary genomics of the cold-adapted diatom *Fragilariopsis cylindrus*, *Nature*, 541, 536–540, doi:10.1038/nature20803, 2017.
- Morris, C. E., Sands, D. C., Bardin, M., Jaenicke, R., Vogel, B., Leyronas, C., Ariya, P. A., and Psenner, R.: Microbiology
715 and atmospheric processes: research challenges concerning the impact of airborne micro-organisms on the atmosphere and climate, *Biogeosciences*, 8, 17–25, doi:10.5194/bg-8-17-2011, 2011.
- Murray, B. J., O'Sullivan, D., Atkinson, J. D., and Webb, M. E.: Ice nucleation by particles immersed in supercooled cloud droplets, *Chemical Society reviews*, 41, 6519–6554, doi:10.1039/c2cs35200a, 2012.
- Olenina, I., Hajdu, S., Edler, L., Andersson, A., Wasmund, N., Busch, S., Göbel, J., Gromisz, S., Huseby, S., Huttunen, M.,
720 Jaanus, A., Kokkonen, P., Ledaine, I., and Niemkiewicz, E.: Biovolumes and size-classes of phytoplankton in the Baltic Sea, *HELCOM Balt.Sea Environ. Proc.*, 106, 2006.
- O'Sullivan, D., Murray, B. J., Ross, J. F., Whale, T. F., Price, H. C., Atkinson, J. D., Umo, N. S., and Webb, M. E.: The relevance of nanoscale biological fragments for ice nucleation in clouds, *Scientific reports*, 5, 8082, doi:10.1038/srep08082, 2015.
- 725 Pinti, V., Marcolli, C., Zobrist, B., Hoyle, C. R., and Peter, T.: Ice nucleation efficiency of clay minerals in the immersion mode, *Atmos. Chem. Phys.*, 12, 5859–5878, doi:10.5194/acp-12-5859-2012, 2012.



- Poulin, M., Daugbjerg, N., Gradinger, R., Ilyash, L., Ratkova, T., and Quillfeldt, C. von: The pan-Arctic biodiversity of marine pelagic and sea-ice unicellular eukaryotes: a first-attempt assessment, *Mar Biodiv*, 41, 13–28, doi:10.1007/s12526-010-0058-8, 2011.
- 730 Pummer, B. G., Bauer, H., Bernardi, J., Bleicher, S., and Grothe, H.: Suspensible macromolecules are responsible for ice nucleation activity of birch and conifer pollen, *Atmos. Chem. Phys.*, 12, 2541–2550, doi:10.5194/acp-12-2541-2012, 2012.
- Pummer, B. G., Budke, C., Augustin-Bauditz, S., Niedermeier, D., Felgitsch, L., Kampf, C. J., Huber, R. G., Liedl, K. R., Loerting, T., Moschen, T., Schauer, M., Tollinger, M., Morris, C. E., Wex, H., Grothe, H., Pöschl, U., Koop, T., and
735 Fröhlich-Nowoisky, J.: Ice nucleation by water-soluble macromolecules, *Atmos. Chem. Phys.*, 15, 4077–4091, doi:10.5194/acp-15-4077-2015, 2015.
- Rasmussen, D. H. and MacKenzie, A. P.: Effect of Solute on Ice-Solution Interfacial Free Energy; Calculation from Measured Homogeneous Nucleation Temperatures, in: *Water Structure at the Water-Polymer Interface*, Springer, Boston, MA, 126–145, 1972.
- 740 Reicher, N., Segev, L., and Rudich, Y.: The Weizmann Supercooled Droplets Observation on a Microarray (WISDOM) and application for ambient dust, *Atmos. Meas. Tech.*, 11, 233–248, doi:10.5194/amt-11-233-2018, 2018.
- Riechers, B., Wittbracht, F., Hütten, A., and Koop, T.: The homogeneous ice nucleation rate of water droplets produced in a microfluidic device and the role of temperature uncertainty, *Physical chemistry chemical physics PCCP*, 15, 5873–5887, doi:10.1039/c3cp42437e, 2013.
- 745 Roy, P., Mael, L. E., Hill, T. C. J., Mehndiratta, L., Peiker, G., House, M. L., DeMott, P. J., Grassian, V. H., and Dutcher, C. S.: Ice Nucleating Activity and Residual Particle Morphology of Bulk Seawater and Sea Surface Microlayer, *ACS Earth Space Chem.*, 5, 1916–1928, doi:10.1021/acsearthspacechem.1c00175, 2021.
- Roy-Barman, M. and Jeandel, C.: *Marine Geochemistry*, Oxford University Press, 2016.
- Šantl-Temkiv, T., Lange, R., Beddows, D., Rauter, U., Pilgaard, S., Dall'Osto, M., Gunde-Cimerman, N., Massling, A., and
750 Wex, H.: Biogenic Sources of Ice Nucleating Particles at the High Arctic Site Villum Research Station, *Environmental science & technology*, 53, 10580–10590, doi:10.1021/acs.est.9b00991, 2019.
- Šantl-Temkiv, T., Sikoparija, B., Maki, T., Carotenuto, F., Amato, P., Yao, M., Morris, C. E., Schnell, R., Jaenicke, R., Pöhlker, C., DeMott, P. J., Hill, T. C. J., and Huffman, J. A.: Bioaerosol field measurements: Challenges and perspectives in outdoor studies, *Aerosol Science and Technology*, 54, 520–546, doi:10.1080/02786826.2019.1676395, 2020.
- 755 Steinke, I., DeMott, P. J., Deane, G. B., Hill, T. C. J., Maltrud, M., Raman, A., and Burrows, S. M.: A numerical framework for simulating the atmospheric variability of supermicron marine biogenic ice nucleating particles, *Atmos. Chem. Phys.*, 22, 847–859, doi:10.5194/acp-22-847-2022, 2022.
- Vance, T. D. R., Bayer-Giraldi, M., Davies, P. L., and Mangiagalli, M.: Ice-binding proteins and the 'domain of unknown function' 3494 family, *The FEBS journal*, 286, 855–873, doi:10.1111/febs.14764, 2019.



- 760 Wagner, R., Ickes, L., Bertram, A. K., Els, N., Gorokhova, E., Möhler, O., Murray, B. J., Umo, N. S., and Salter, M. E.:
Heterogeneous ice nucleation ability of aerosol particles generated from Arctic sea surface microlayer and surface seawater
samples at cirrus temperatures, *Atmos. Chem. Phys.*, 21, 13903–13930, doi:10.5194/acp-21-13903-2021, 2021.
- Welti, A., Bigg, E. K., DeMott, P. J., Gong, X., Hartmann, M., Harvey, M., Henning, S., Herenz, P., Hill, T. C. J., Hornblow,
B., Leck, C., Löffler, M., McCluskey, C. S., Rauker, A. M., Schmale, J., Tatzelt, C., van Pinxteren, M., and Stratmann,
765 F.: Ship-based measurements of ice nuclei concentrations over the Arctic, Atlantic, Pacific and Southern oceans, *Atmos.*
Chem. Phys., 20, 15191–15206, doi:10.5194/acp-20-15191-2020, 2020.
- Wex, H., Augustin-Bauditz, S., Boose, Y., Budke, C., Curtius, J., Diehl, K., Dreyer, A., Frank, F., Hartmann, S., Hiranuma,
N., Jantsch, E., Kanji, Z. A., Kiselev, A., Koop, T., Möhler, O., Niedermeier, D., Nillius, B., Rösch, M., Rose, D., Schmidt,
C., Steinke, I., and Stratmann, F.: Intercomparing different devices for the investigation of ice nucleating particles using
770 Snomax® as test substance, *Atmos. Chem. Phys.*, 15, 1463–1485, doi:10.5194/acp-15-1463-2015, 2015.
- Wilson, T. W., Ladino, L. A., Alpert, P. A., Breckels, M. N., Brooks, I. M., Browse, J., Burrows, S. M., Carslaw, K. S.,
Huffman, J. A., Judd, C., Kilthau, W. P., Mason, R. H., McFiggans, G., Miller, L. A., Nájera, J. J., Polishchuk, E., Rae,
S., Schiller, C. L., Si, M., Temprado, J. V., Whale, T. F., Wong, J. P. S., Wurl, O., Yakobi-Hancock, J. D., Abbatt, J. P.
D., Aller, J. Y., Bertram, A. K., Knopf, D. A., and Murray, B. J.: A marine biogenic source of atmospheric ice-nucleating
775 particles, *Nature*, 525, 234–238, doi:10.1038/nature14986, 2015.
- Wolber, P. K., Deininger, C. A., Southworth, M. W., Vandekerckhove, J., van Montagu, M., and Warren, G. J.: Identification
and Purification of a Bacterial Ice-Nucleation Protein, *Proceedings of the National Academy of Sciences of the United
States of America*, 83, 7256–7260, 1986.
- Xi, Y., Mercier, A., Kuang, C., Yun, J., Christy, A., Melo, L., Maldonado, M. T., Raymond, J. A., and Bertram, A. K.:
780 Concentrations and properties of ice nucleating substances in exudates from Antarctic sea-ice diatoms, *Environmental
science. Processes & impacts*, 23, 323–334, doi:10.1039/d0em00398k, 2021.